IOP Publishing Journal of Physics: Condensed Matter
J. Phys.: Condens. Matter **32** (2020) 195701 (14pp) https://doi.org/10.1088/1361-648X/ab6d0e

Dual-doped CdSe:Cu:O films grown by sputtering using CdSe–CuO composite targets

Ninfa Navarro López[1], Francisco Rodríguez-Melgarejo[1], Martín Hernández-Landaverde[1], Francisco Javier Flores-Ruiz[2] and Sergio Jiménez-Sandoval[1]

[1] Centro de Investigación y de Estudios Avanzados del IPN, Unidad Querétaro, Libramiento Norponiente No. 2000, Frac. Real de Juriquilla, Querétaro, Qro. C.P. 76230, Mexico
[2] Conacyt-Instituto de Física, Benemérita Universidad Autónoma de Puebla, Apdo. Postal J-48, Puebla Pue. 72570, Mexico

E-mail: sergio.jimenez@cinvestav.mx

Received 6 September 2019, revised 4 January 2020
Accepted for publication 17 January 2020
Published 13 February 2020

Abstract

The effects of the simultaneous incorporation of Cu and O in CdSe films grown by sputtering are presented. The Cu and O contents varied between 1 and 5 at.% in films deposited at 150, 200, 250 and 300 °C. Concentrations of 2, 3, 4 and 5 at.% of CuO in the target promoted the formation of copper selenide clusters immersed within the CdSe:Cu:O host. Energy considerations (enthalpy of formation and bond dissociation energy) were used to discuss the absence of copper oxide and the formation of copper selenide aggregates, as well as the film thickness dependence on the concentration of CuO in the target. The band gap of the films ranged from 1.21 to 2.07 eV, depending upon growth conditions. Significant below-band-gap absorption was observed which was ascribed to the copper selenide micro and nano clusters. Good crystalline quality of the films, for high substrate temperatures, was evidenced through the appearance of overtones of the vibrational longitudinal optic modes detected by Raman micro spectroscopy. It was determined that the electronic properties, optical transmission and electrical conductivity depended on the chemical composition and crystalline structure. This characteristic is relevant because through copper and oxygen co-doping is possible to control these technologically important physical properties of CdSe in a simple and reliable manner.

Keywords: semiconductors, solid solutions, electronic properties, thin film growth

(Some figures may appear in colour only in the online journal)

1. Introduction

The study of semiconductor materials based on II–VI compounds has been extensive in recent years given their applicability in opto-electronic devices. Some of their major advantages of these materials include their excellent opto-electronic properties, with high optical absorption coefficients, and their favorable band gap (E_g) for solar energy conversion [1]. In particular, cadmium selenide (CdSe) is a semiconductor material of great interest due to its wide range of applications in solid state devices such as thin film transistors and photovoltaic cells [2]. Its band gap (1.70 eV) is appropriate for achieving high efficiencies in solar-cell devices. Diverse techniques have been used in the past for the deposition of CdSe films. Among them, one can mention chemical vapor [3] and pulsed laser deposition [4], thermal evaporation [5] and radio frequency sputtering [6]. The sputtering technique has the advantage of controlling thickness and dopant concentration with relative ease. In addition, reproducibility and homogeneity are also common characteristics of sputtered films.

The modification of properties of CdSe films upon the incorporation of different dopants such as Cu, O, Bi, Sb and

Fe has been the subject of previous reports. A crystallite size increase in CdSe:Cu films along with a concomitant band gap reduction [7], while the effect of copper in the emission of CdSe quantum dots have been reported [8]. Zheng *et al* studied the incorporation of oxygen in CdSe films. Samples with high oxygen contents showed a remarkable amorphization and the appearance of diffraction peaks associated with SeO_2 [9]. Santhosh *et al* reported an increase in the conductivity associated to the concentration of Bi in the samples, with no significant changes in the band gap [10]. A similar behavior in the band gap was observed in Sb-doped CdSe films, where the hexagonal crystalline structure was not modified upon dopant incorporation [5].

The electronic properties of a related chalcogenide, cadmium telluride (CdTe), have been successfully modified through dual-doping with copper and oxygen. This approach has proven to be a successful way for controlling the optical and electrical properties of CdTe by appropriate choice of Cu and O concentrations [11, 12]. Along this line of work, the structural, optical and electrical properties of films grown from ZnSe–Cu_2O composite sputtering targets were also studied [13]. The investigation of the properties in CdSe based materials is an important step in the search for new materials whose physical properties could be tailored. Dual-doping is an interesting approach to control the physical properties of II–VI compounds. The use of composite targets has proven to be a simple and robust method for growing doped semiconductor films [14–16]. In this work the structural, optical and electrical properties of CdSe sputtered films are reported for the first time, using different concentrations of CuO (as source of Cu and O atoms) in the sputtering target and for different substrate temperatures. Our results show that the electronic properties of CdSe can be readily modified through dual-doping with copper and oxygen.

2. Experimental

The films were deposited by the radio frequency sputtering on Corning glass substrates. The cleaning process included submerging in a highly concentrated chromic acid for 24 h to remove impurities adhered to the substrate surface and improve adhesion of the films. A two-inch diameter target was made by compacting mixtures of CdSe (Aldrich, 99.99%) and CuO (ESPI, 99.99%) powders. The CuO concentrations in the target were 1, 2, 3, 4 and 5 at.%. For comparison purposes, a CdSe:Cu target was made with a copper concentration of 2 at.%. During growth an argon flow of 15 sccm was maintained in the chamber, with a radio frequency power of 50 W applied to the target. The substrate-to-target distance was 8 cm and the substrate temperature (T_s) varied from 150 to 300 °C for different runs. The targets were pre-sputtered for five minutes, followed by the deposition of the films for 60 min, under a working pressure of ~4.5–5.5 $\times$ 10^{-3} Torr. The base pressure reached by the pumping system was ~2 $\times$ 10^{-5} Torr.

X-ray diffraction studies were performed in a Rigaku D/Max-2100 diffractometer using the Cu k_α line (1.5406 Å) in the 2θ range of 10–70°. Inelastic light scattering experiments were carried out in a HORIBA micro Raman spectrometer model HR Evolution using a He-Ne laser (632.8 nm), as excitation source, focused on the sample surface with the help of a 50 $\times$ objective. The optical transmission spectra were measured at normal incidence in a Cary 5000 spectrometer from Agilent Technologies in the wavelength range from 300 to 3300 nm. The resistivity was obtained in a four-point probe resistance meter T600 Lorest-GP. The thickness of each film was measured using a mechanical profilometer Sloan Dektak II. The surface roughness of the films was measured using a Bruker Dimension Edge atomic force microscope (AFM). The composition of the films was estimated in films deposited on Si substrates from energy dispersive spectroscopy (EDS) using a scanning electron microscope XL30 ESEM, Phillips.

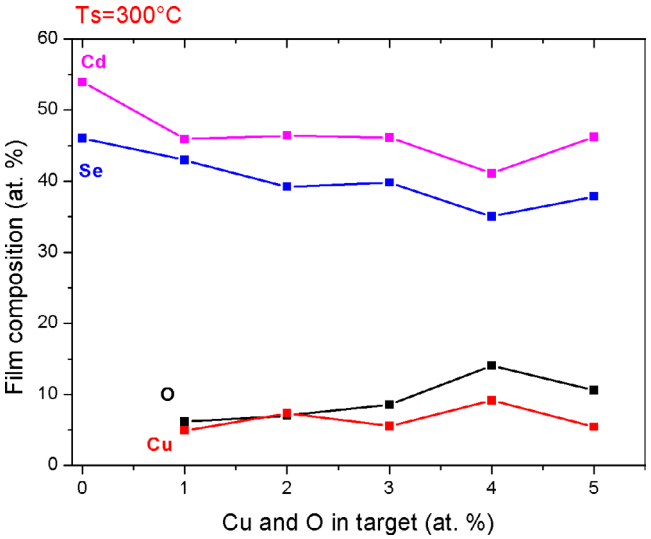

Figure 1. Chemical composition of the films deposited at 300 °C as a function of the concentration of CuO in the target.

3. Results and discussion

3.1. Films composition

The chemical composition of the films was determined from EDS measurements. For these measurements, a piece of a silicon wafer was placed on top of the glass slide substrate for each deposition. This was done basically to avoid any contribution from oxygen originating from the glass substrates. In all cases, only the expected chemical constituents were observed, that is, no undesired impurities were present in the films. In what follows, the results for some representative cases are presented and discussed. Figure 1 shows the chemical composition for the samples grown at 300 °C as a function of nominal concentration of CuO in the target, including the composition of the undoped CdSe film. A general feature is that the concentration of Cd is larger than that of Se, even for the undoped CdSe film. The loss of selenium is consistent with its large vapour pressure, and its loss produced by the continuous pumping of the chamber during depositions. As expected, there is an increase of Cu and O concentrations, as the contents of CuO in the target was raised, figure 1. Figures 2(a) and (b) show the chemical composition of the films with 4

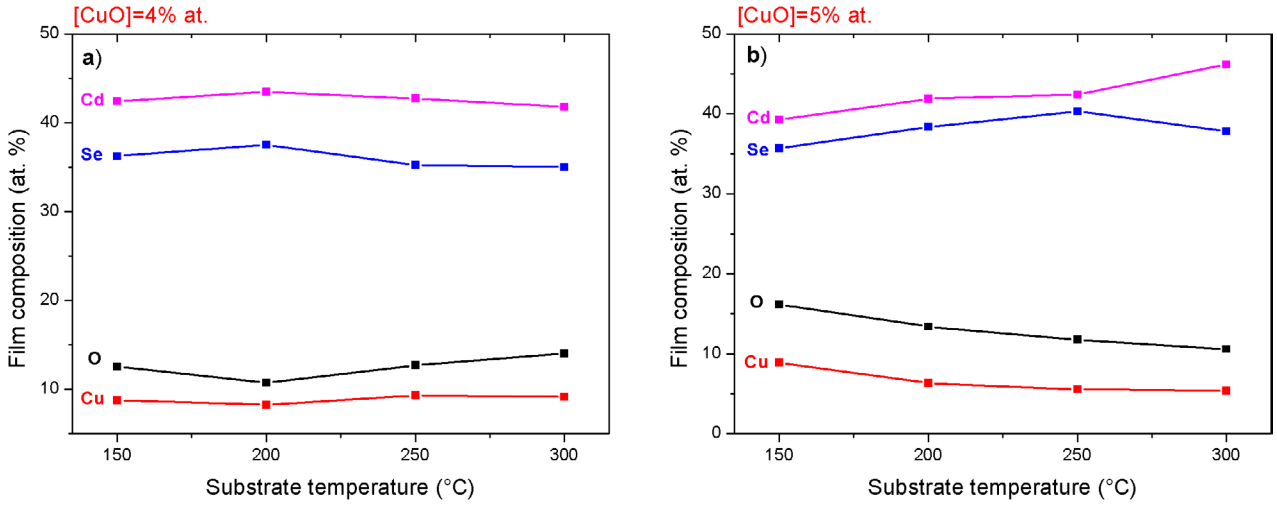

Figure 2. Chemical composition of the films as a function of the substrate temperature for the CuO concentration of (a) 4 at.% and (b) 5 at.% in the target.

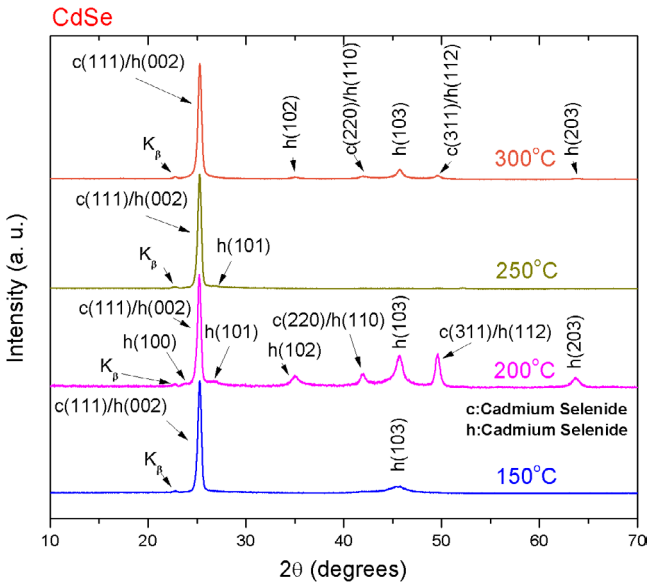

Figure 3. Diffraction patterns of CdSe films deposited at different substrate temperatures. Reflections from cubic (*c*) and hexagonal (*h*) planes are indicated for each case. Due to the high intensity of the main peak, the reflection originated by the k_β emission of the x-ray source (Cu) is observable.

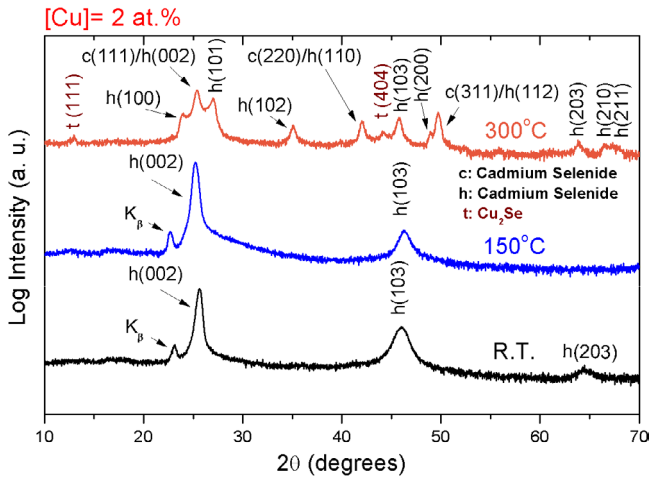

Figure 4. Diffraction patterns of CdSe:Cu (2 at.%) films deposited at different substrate temperatures. Note the logarithmic scale for the intensity.

and 5 at.% of CuO, as a function of the substrate temperature. As observed, the chemical composition of the films when [CuO] = 4 at.% does not vary significantly as the substrate temperature changed. This observation no longer holds when [CuO] = 5 at.%, since a small variation in chemical composition occurred. In general, the concentration of Cu and O follow the same trend in all films, with a somewhat larger value for oxygen. This may be caused by the incorporation during growth of residual oxygen in the chamber. In summary, the EDS analysis showed peaks related to Cd, Cu, Se, O and of some residual carbon. The carbon signal originated from residual contamination in the chamber [17]. Up to the detection limits of EDS, no undesired impurities were present in the films.

3.2. Structural characterization

The x-ray diffraction patterns of pure CdSe films are shown in figure 3. The films are polycrystalline and have sharp peaks associated with the cubic phase (CdSe, JCPDS No. 19-0191) and hexagonal (cadmoselite, JCPDS No. 08-0459) of CdSe, phases labeled as *c* and *h*, respectively. The films showed preferential orientation parallel to the planes *h*(0 0 2)/*c*(1 1 1). This dominant orientation has been reported as well in films deposited by vacuum deposition techniques [18], electron beam evaporation [19] and chemical vapor deposition [20]. The film deposited at $T_s = 150$ °C presented a high intensity peak related to *h*(0 0 2)/*c*(1 1 1) planes and one of lower intensity corresponding to (1 0 3) reflections. When T_s is increased to 200 °C, more texture was observed through the appearance of planes (1 0 1), (1 0 2), (1 1 0), (1 1 2) and (2 0 3) of the hexagonal phase. These planes were also observed in the film deposited at 300 °C. In the case of $T_s = 250$ °C, only the planes *h*(0 0 2)/*c*(1 1 1) and (1 0 1) were detected. One general characteristic of the diffraction patterns in figure 3 is their large

Table 1. Crystallite size, lattice and microstructural parameters for CdSe, CdSe:Cu and CdSe:Cu:O films deposited at different substrate temperatures (T_s), d_{002} indicates the interplanar distance between the (0 0 2) planes.

	T_s (°C)	2θ, (0 0 2) peak (degrees)	d_{002} (Å)	FWHM (0 0 2) peak	Crystallite size (nm)	Strain[c] ($\times 10^{-3}$)	Dislocation density ($\times 10^{15}$ lines m^{-2})
CdSe	150	25.25	3.52	0.416	20.4	24.74	7.17
	200	25.22	3.53	0.406	20.9	4.52	6.81
	250	25.23	3.52	0.417	20.4	−2.52	7.20
	300	25.27	3.52	0.409	20.8	17.84	4.68
CdSe:Cu 2 at.%	R.T.	25.63	3.47	0.478	17.8	2.50	9.45
	150	25.17	3.53	0.499	17.0	39.83	10.32
	300	25.27	3.52	1.137	7.5	50.10	53.61
CdSe:Cu:O 1 at.%	150	25.06	3.55	16.761	[b]	[a]	[b]
	200	24.24	3.67	14.656	[b]	[a]	[b]
	250	25.18	3.53	1.028	8.3	−13.18	43.86
	300	25.15	3.54	0.980	8.7	−13.33	39.81
CdSe:Cu:O 2 at.%	150	24.49	3.63	12.078	[b]	[a]	[b]
	200	25.09	3.54	1.249	6.8	−24.41	64.68
	250	25.54	3.48	0.671	12.3	16.98	19.8
	300	25.36	3.51	0.704	12.1	21.16	20.52
CdSe:Cu:O 3 at.%	150	24.94	3.56	0.616	13.8	−3.45	15.75
	200	25.39	3.50	0.617	13.8	23.98	15.75
	250	25.40	3.50	0.730	11.7	−4.18	22.05
	300	45.66	1.98	0.459	19.6	−19.75	7.77
CdSe:Cu:O 4 at.%	150	24.83	3.58	0.603	14.1	85.78	15.06
	200	24.74	3.59	0.765	11.1	[a]	24.30
	250	25.37	3.51	0.778	10.9	[a]	25.05
	300	25.56	3.48	0.734	11.6	3.51	22.29
CdSe:Cu:O 5 at.%	150	24.88	3.57	0.622	13.7	81.50	16.05
	200	25.39	3.50	0.741	11.5	[a]	22.74
	250	25.37	3.51	0.804	10.6	4.54	26.79
	300	25.26	3.52	0.656	13.0	−19.59	17.82

[a] Values omitted due to inconsistent fit for Williamson–Hall method.
[b] Values omitted for amorphous films.
[c] Positive (negative) values indicate tensile (compressive) strain.

signal-to-noise (S/N) ratio, which is maintained in most of the doped samples. In fact, in figures 4 and 6, a logarithmic scale was used so that the lower intensity peaks could be noticeable.

Table 1 lists the crystallite size and lattice parameters for the CdSe films along with those of the CdSe:Cu and CdSe:Cu:O samples. The interplanar distance d was calculated with the help of Bragg's law [21],

$$2d \sin\theta = n\lambda \tag{1}$$

where λ is the wavelength of the x-ray beam. The crystallite size of the films was estimated using the Scherrer's formula [21]:

$$D = \frac{k\lambda}{\beta \cos\theta} \tag{2}$$

where k is the Scherrer constant with a value of 0.9, β is the full width at half maximum (FWHM) of the most intense peak in radians, and θ the diffraction angle.

The crystallite size for the CdSe samples was around ~20 nm regardless of the substrate temperature. Mathuri *et al* reported small crystallite size variations (from ~19.69 to ~23.10 nm) for CdSe films deposited at different substrate temperatures [19]. There is no significant variation in the values of the interplanar distance of the planes $h(0\,0\,2)/c(1\,1\,1)$ for the CdSe films. The calculated values for this distance (~3.52 Å) are in good agreement with those reported for CdSe films (3.517 Å) [18].

The strain of the films ε, table 1, was estimated using the Williamson–Hall method, through of the following relation [22]:

$$\beta \cos\theta = \left(\frac{k\lambda}{D}\right) + 4\varepsilon \sin\theta \tag{3}$$

where β is the full width at half maximum, and θ the diffraction angle of the considered peak. When the term ($\beta\cos\theta$) is plotted against ($4\sin\theta$) for the peaks at 2θ in a diffraction pattern, the value of the slope of the linear fit corresponds to the strain in the sample. The sign of the strain may be positive or negative, which correspond to tensile or compressive strain [22], table 1.

The dislocation density was estimated through the Williamson and Smallman's relation [23]. Based on experimental data, Williamson and Smallman applied a model to determine the dislocation density in various metals. Microbeam experiments indicated that these materials could be considered as divided into a series of blocks, separated by

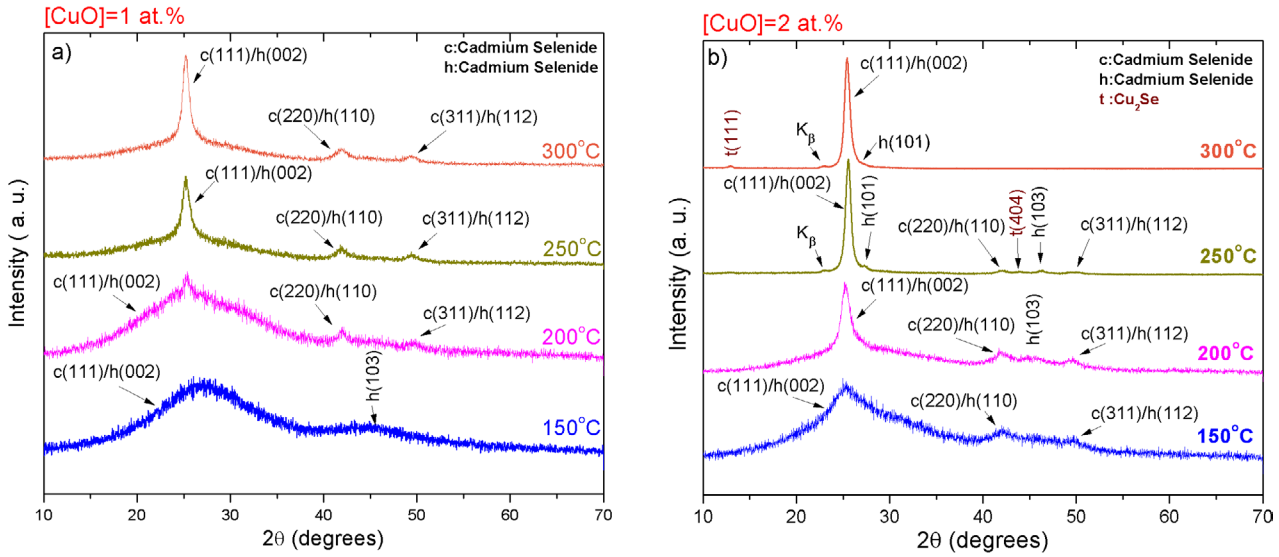

Figure 5. Diffraction patterns of CdSe:Cu:O films deposited at different substrate temperatures for different concentrations of CuO in the target: (a) 1 and (b) 2 at.%.

dislocations which were the actual boundaries between the blocks. If there are n dislocations per block face, the total length of the dislocation line per block is $6nD/2$ (since each face is shared by 2 blocks) where D is the dimension of the block. The number of blocks per unit volume is $1/D^3$ and, therefore, the dislocation density calculated from the crystallite size is:

$$\rho = \frac{6nD}{2D^3} = \frac{3n}{D^2}. \tag{4}$$

To use this equation, the value of n must be determined, or assumed. The value of $n = 1$ is usually employed to estimate a *minimum* for the dislocation density of different types of materials [5, 24, 25]. The values of dislocation densities given in table 1 were obtained using the relation $3/D^2$. Strain and dislocation density of 1.98×10^{-3} and 22.24×10^{14} lines m^{-2} were reported previously for CdSe films [26], respectively. Similarly, Ahamed *et al* reported values for strain of 1.82×10^{-3} and a dislocation density of 21.2×10^{14} lines m^{-2} [27].

The crystallite size, FWHM and interplanar distance d_{002} were calculated for hexagonal CdSe using the most intense peak, i.e. that of preferential orientation. In general, the largest crystallite sizes and lowest values for strain and dislocation density were obtained for undoped CdSe films, table 1.

To begin the analysis of the doped samples, the case of introducing only copper as dopant is considered (as opposed to dual Cu–O doping). Figure 4 shows the x-ray diffraction patterns of the CdSe:Cu films (2 at.% of copper) deposited at RT, 150 and 300 °C (with logarithmic scale in the intensity axis). These patterns indicate that the films are polycrystalline oriented preferentially. The films grown at RT and 150 °C did not show any cubic-related peaks. Most of the peaks for the film grown at $T_s = 300$ °C correspond to the hexagonal phase of cadmium selenide, in addition to weak peaks corresponding to tetragonal copper selenide (labeled as t-Cu_2Se). These results show that the substrate temperature is an important parameter for crystalline phase control and, therefore, to determine the physical properties. The crystallite sizes for these samples are smaller as compared to those of undoped CdSe films. From table 1 it may be observed that sizes for the copper-doped films varied between 17.81 (RT) and 7.48 nm (300 °C). Concomitantly with the crystallite size reduction upon copper doping, in general the strain and dislocation density were larger than those of the undoped films, table 1.

The diffraction patterns for CdSe:Cu:O films for different substrate temperatures with concentrations of 1 and 2 at.% of CuO in the target are shown in figure 5. In the case of 1 at.%, figure 5(a), the results show that for $T_s = 150$ °C the films are amorphous. At 200 °C some crystallization occurred but the diffractogram is still dominated by amorphous-related features. As the substrate temperature was raised to 250 °C and 300 °C, crystallinity improved. As in the previous cases, the most intense peak corresponds to the $h(0\,0\,2)/c(1\,1\,1)$ planes. When comparing the diffraction patterns of undoped CdSe films with those of the samples with 1 and 2 at.% of CuO, it is noted the effect of the incorporation of CuO in the crystalline structure. Upon doping, the films were structurally disordered, which decreased as substrate temperatures were set at higher values. In this direction, it was reported that in the case of CdSe:O films grown by pulsed laser deposition, by increasing the oxygen pressure in the chamber crystallinity was suppressed [9]. In a similar effect, oxygenation of sputtered CdTe films induced an amorphous state in the films [28, 29]. These results are in correspondence with the observed behavior in the CdSe:Cu:O films; however, due to the Cu:O dual-doping some differences exist. When incorporating CuO in the target, low-temperature films exhibit amorphous structure. In contrast, even the CdSe:Cu film grown at room temperature is polycrystalline, figure 4. These observations evidence that the structural disorder in the co-doped films is induced by the presence of oxygen. Correspondingly, Cu:O co-doping produced a decrease in crystallite size, table 1. It is interesting the difference in growth habits between the

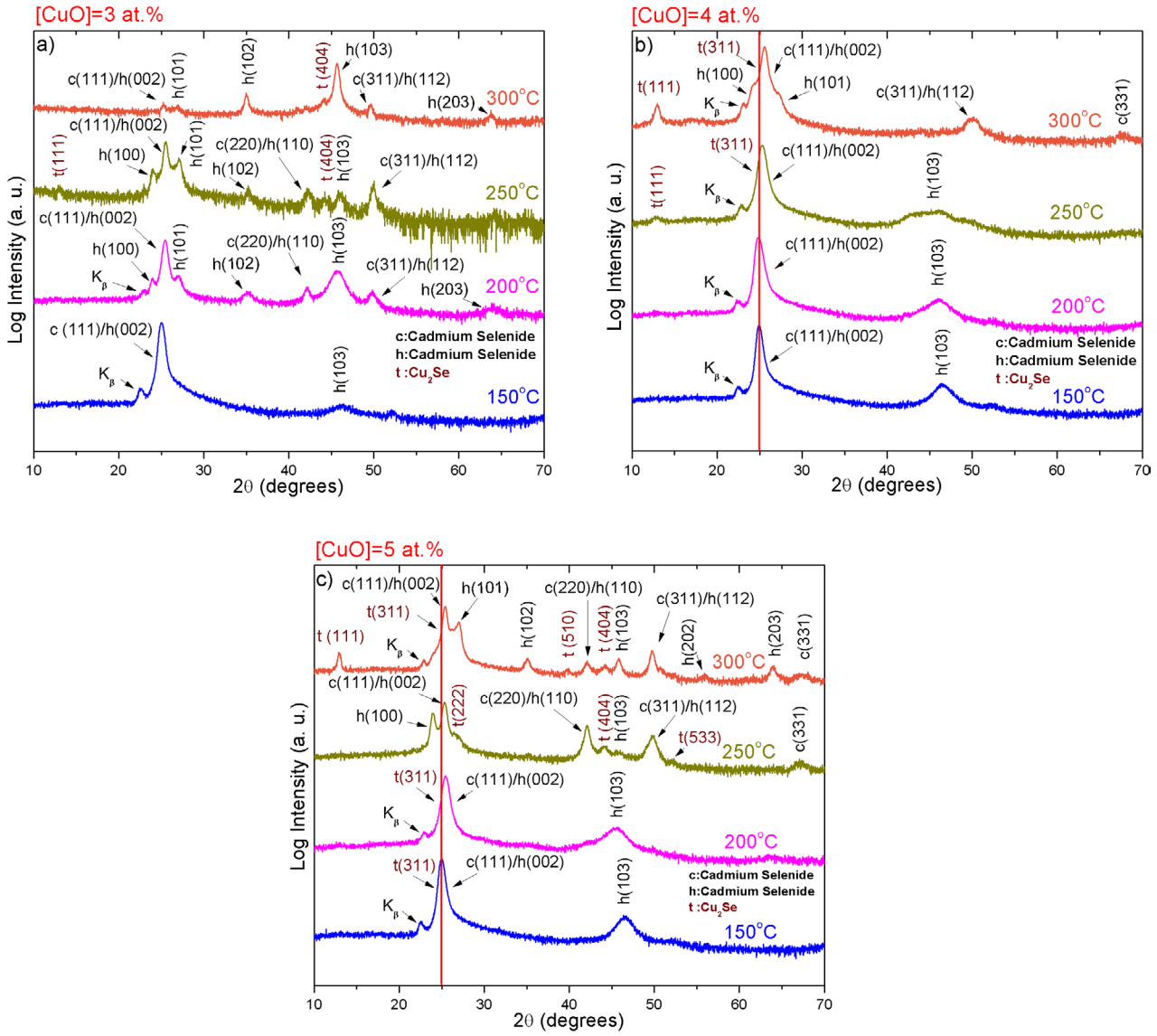

Figure 6. Diffraction patterns of CdSe:Cu:O films deposited at different substrate temperatures: (a) 3, (b) 4 and (c) 5 at.%. Note the logarithmic scale for the intensity.

CdSe:Cu (figure 4) and the CdSe:Cu:O (figure 5) films, which shows that the growth dynamics are remarkably different when CdSe growths are accompanied by Cu atoms, or when Cu and O atoms are simultaneously incorporated in the lattice.

Figure 6 presents the diffraction patterns of the CdSe films with concentrations in the target of [CuO] = 3, 4, and 5 at.%. In the 3 percent case, figure 6(a), phase segregation is observable for films with $T_s \geqslant 250$ °C through the appearance of Cu_2Se aggregates. As in the previous cases, the presence of peaks corresponding to the cubic and hexagonal phases of CdSe are noticeable as well. The films showed preferential growth for the planes $h(0\,0\,2)/c(1\,1\,1)$ when $T_s \leqslant 250$ °C; while for $T_s = 300$ °C the hexagonal (1 0 3) planes were favored. In the case of [CuO] = 4 at.% the appearance of the Cu_2Se phase occurs at $T_s = 250$ °C. All films have a preferential orientation along the plane $h(0\,0\,2)/c(1\,1\,1)$, figure 6(b). At concentrations of [CuO] = 5 at.%, figure 6(c), several peaks appear associated to the Cu_2Se phase for $T_s = 250$ and 300 °C. The formation of copper selenide aggregates indicates that during the sputtering process of the composed CdSe–CuO targets, a dissociation of CdSe and CuO particles occurred so that Cu–Se bonds form during the growth process. In fact, x-ray diffraction showed that for the higher substrate temperatures (250 °C–300 °C) and pressure (a few mTorr), the formation of copper selenide was substantially favored. No copper oxide was observed in our measurements. The standard molar enthalpies of formation ($\Delta_f H^o$) of CuO and CuSe are −157.3 and −39.5 kJ mol^{-1}, respectively [30]. That is, thermodynamically the formation of Cu–O bonds represents a state of lower energy than those of Cu–Se; however, our growth conditions yielded preferentially the latter. At this point it is convenient to recall that the quoted values of $\Delta_f H^o$ given above were obtained at standard conditions $T = 298.15$ K and $P = 1$ bar, which are significantly different from those in the sputtering chamber during growth ($T > 448$ K, $P \sim 10^{-6}$ bar). Otherwise stated, the experimental evidence shows that the dynamics of the out-of-equilibrium sputtering process, and the particular values of substrate temperature and pressure in the chamber

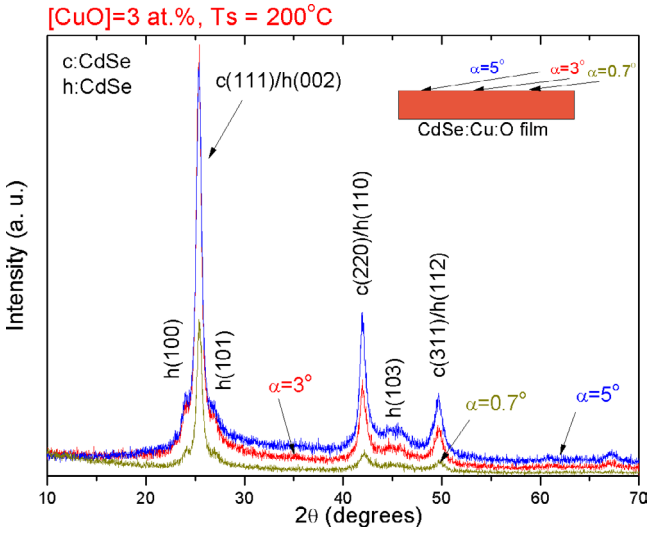

Figure 7. Diffraction pattern of CdSe:Cu:O (3 at.%) films deposited at 200 °C, measured at incidence angles of $\alpha = 0.7°$, 3° y 5°.

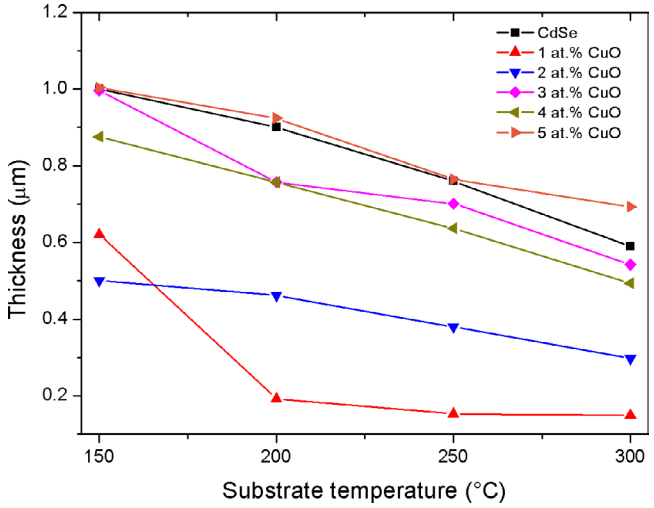

Figure 8. Film thicknesses of CdSe, CdSe:Cu:O (1, 2, 3, 4 y 5 at.%) as a function of substrate temperature.

favored the formation of Cu–Se bonds. Moreover, the standard molar enthalpies of formation of other possible oxides, namely, SeO_2 and CdO are −109.62 and −258.2 kJ mol^{-1}, respectively, thus a similar comment would apply in regard to the non-observation of these compounds and the favored formation of Cu_2Se. It should be mentioned, however, that the fact that we did not detect any of the above-mentioned oxides, though, does not rule out their presence in the samples in the form of amorphous or nanocrystalline phases.

To determine the structural in-depth homogeneity of the films, grazing-angle x-ray diffraction measurements were carried out for various angles of incidence (α) of the x-ray beam. Thus, different depths could be probed. Three incidence angles were used: 0.7, 3 and 5°, measured with respect to the surface of the film, as shown in the inset in figure 7. The diffraction patterns for all angles were similar with no significant variations in the peaks' positions or relative intensities. Figure 7 shows the patterns for the film with [CuO] = 3 at.% in the target and $T_s = 200$ °C. As it may be observed, the diffractograms show the same peaks with similar relative intensities, indicating that the phases formed are evenly distributed throughout the volume of the film.

In figure 8 are plotted the films´ thicknesses as a function of substrate temperature for CuO concentrations in the target of 1, 2, 3, 4 and 5 at.% and for the undoped CdSe films. Two trends can be noticed: (i) the thickness decreases as the concentration of CuO in the target increases; and (ii) when the substrate temperature is higher, the thickness of the films is smaller. The former (i) indicates that the sputtering rate of the target is reduced for higher concentrations of CuO. This can be explained by considering the bond dissociation energies D^o(R-X) of the compounds in the target. For copper oxide D^o(Cu-O) is 287.4 ± 11.6 1/kJ mol^{-1}, more than twice that of D^o(Cd-Se) which is 127.6 ± 25.1 1/kJ mol^{-1}. It takes more than a factor of two more energy to break a Cu–O bond than a Cd–Se bond. Therefore, it is reasonable that the sputtering rate is lower for targets with larger CuO concentrations. The latter (ii), is an expression of the fact that higher substrate temperatures promote ad-atoms re-evaporation from the film surface, thus reducing the final film thickness.

3.3. Atomic force microscopy (AFM)

The root mean square roughness (RMS) of CdSe and CdSe:Cu:O films was determined from AFM images. The results are shown in figures 9(a) and (b) for films deposited at $T_s = 200$ and 300 °C. In both cases, the smallest roughness was obtained for the sample with a concentration of 1 at.% of CuO, while the largest was obtained for the sample with a concentration of 3 at.%. Beyond this concentration the roughness dropped for [CuO] = 4 and 5 at.%. In the case of undoped CdSe films, the roughness was larger for higher substrate temperatures. It increased from 13 nm for $T_s = 200$ °C to 23 nm for $T_s = 300$ °C. The values of roughness obtained in this work are lower than those obtained for films deposited by other techniques such as chemical bath deposition (52.95–73.99 nm) [31] and thermal evaporation (126–452 nm) [32]. A roughness of 14.5 nm was reported for CdSe films deposited by sputtering [36], in agreement with those obtained in this work.

The roughness of the CdSe:Cu film with 2 at.% of copper in the target had similar values. These were 18 and 21 nm for $T_s = 200$ °C and 300 °C, respectively. As an example, in figure 10 the AFM images for four investigated samples deposited under different conditions are presented. Figures 10(a) and (b) correspond to films with a CuO concentration of 1 at.% and $T_s = 200$ and 300 °C, respectively. An increase in grain size can be observed as the substrate temperature was increased. This behavior was also present in films deposited at 200 and 300 °C for [CuO] = 5 at.% (figures 10(c) and (d)).

3.4. Raman spectroscopy

Raman spectroscopy is a non-destructive technique useful to identify the existence of compounds, detect impurities, probe crystalline quality, among other inelastic light scattering

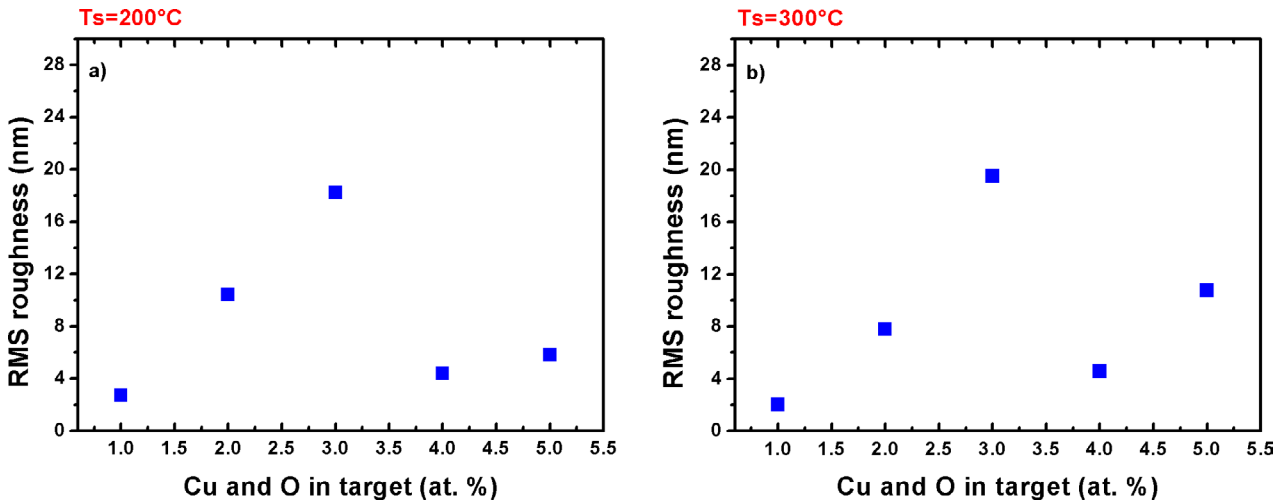

Figure 9. RMS roughness of CdSe:Cu:O films as a function of CuO concentration in the target. The values shown are for films deposited at temperatures of (a) 200 °C and (b) 300 °C.

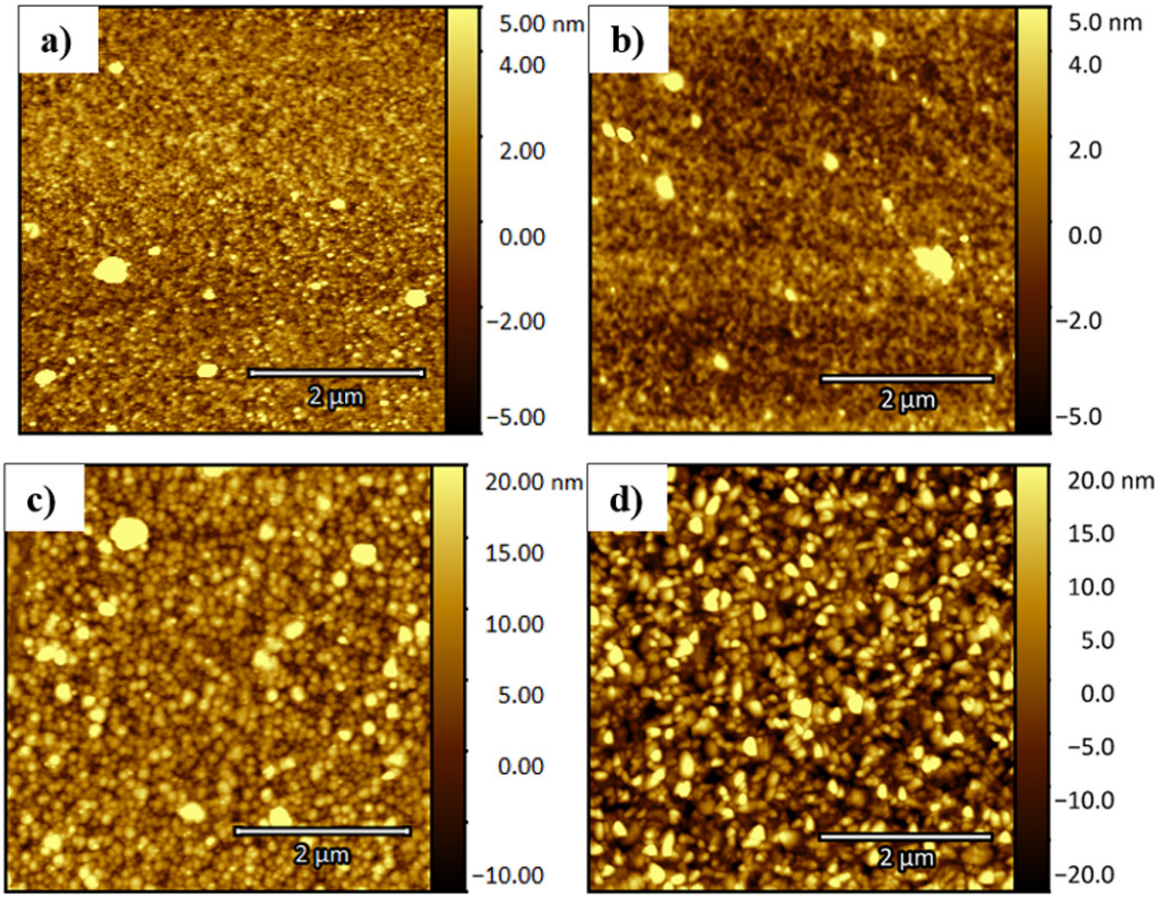

Figure 10. AFM images of CdSe:Cu:O films: (a) [CuO] = 1 at.%, T_s = 200 °C, (b) [CuO] = 1 at.%, T_s = 300 °C, (c) [CuO] = 5 at.%, T_s = 200 °C and (d) [CuO] = 5 at.%, T_s = 300 °C.

processes. In general, this spectroscopy is sensitive to any physical property that affects the long-wavelength vibrational modes in crystalline materials. Cadmium selenide may crystallize in two different structures: cubic-zincblende (ZB) and hexagonal-wurtzite (WZ). In bulk CdSe the ZB phase is stable at low temperature, however, it is transformed into the WZ phase at temperatures above 95 °C [33]. These two crystalline structures have in common tetragonal bonding of any atom to its nearest neighbors. This similarity in the atomic surroundings produces that the frequency of their most intense Raman bands is nearly the same. In particular, the longitudinal optic (LO) frequencies in both crystalline structures nearly coincide. Group theory, however, predicts a different number and symmetry of the Raman active phonons for cubic-ZB and hexagonal-WZ structures. Experimentally, it is particularly difficult to obtain single-phase ZB or WZ CdSe samples. This

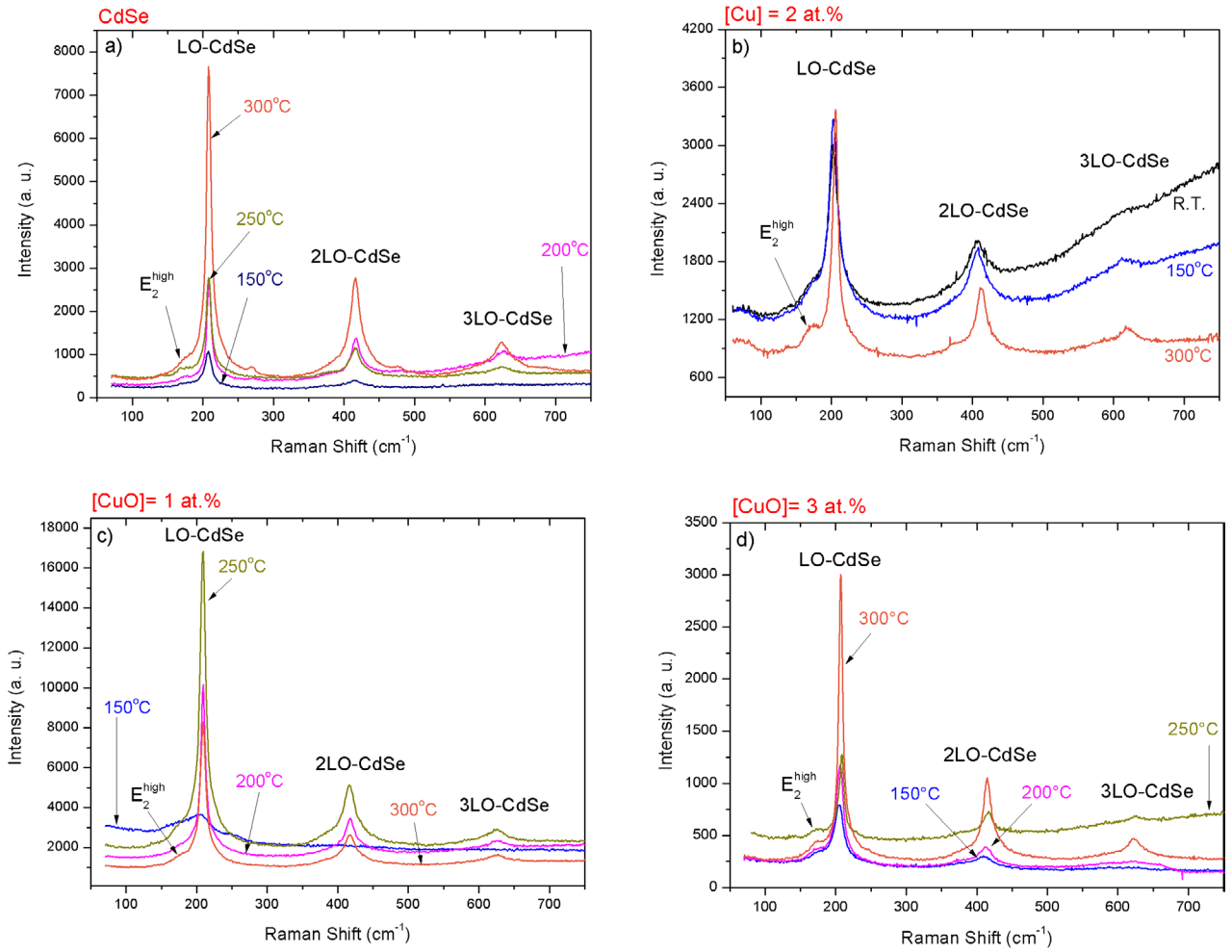

Figure 11. Raman spectra of CdSe and of doped films for different concentrations of Cu and CuO in the target. The slope in the RT and 150 °C spectra in (b) are due to luminescence of the substrate (glass). These films were thinner (~0.80 microns) than the others, thus the laser beam reached the substrate surface.

issue, however, was addressed by Cusco *et al* who carried out Raman scattering studies on high-quality CdSe films deposited by molecular beam epitaxy (MBE) to determine the frequencies of the vibrational modes in single-phase ZB and WZ CdSe [34].

Figure 11 shows the Raman spectra of CdSe, CdSe:Cu ([Cu] = 2 at.%) and CdSe:Cu:O ([CuO] = 1 and 3 at.%) films obtained by using a He–Ne laser (632.8 nm) as excitation source. All spectra show basically the same characteristics: a strong LO mode at ~207 cm^{-1} and its overtone (2LO) at ~416 cm^{-1}. In most cases, a third overtone (3LO) can also be observed at ~ 624 cm^{-1}. The LO mode for the ZB phase of CdSe has been reported at 205.2 cm^{-1}, while for WZ CdSe this mode was observed at 207.2 cm^{-1} for films deposited by molecular beam epitaxy [34]. Other workers reported the frequencies of the LO mode and its first overtone at 209 cm^{-1} and 410 cm^{-1}, respectively [35]. In addition, the E_2^{high} mode is observed in figure 11 at the low-frequency side of the LO band at ~174 cm^{-1}. This mode is characteristic of WZ CdSe. The E_2^{high} mode is clearly visible in the spectrum of sample CdSe:Cu grown at 300 °C (figure 11(b)), which agrees with the dominant presence of peaks related to the hexagonal phase in the diffraction pattern of this sample, figure 4. All the features in the Raman spectra of the films corresponded to CdSe vibrational properties. This indicates that the Raman cross-section of copper selenide is substantially lower than that of CdSe.

3.5. Optical properties

Figure 12 shows the transmission spectra of CdSe and CdSe:Cu for different substrate temperatures. Interference oscillations due to multiple reflections at the air/film and film/substrate interfaces can be observed in the CdSe spectra, figure 12(a). The mean transmittance correlates with the thickness (i.e. lower transmittance for thicker films) and with the surface roughness (rougher surfaces produce larger dispersion of the incident beam light). In the case of CdSe:Cu films, figure 12(b), there is a substantial decrease in the transmittance spectra as the substrate temperature was raised. Not only the overall transmittance was reduced, and the interference oscillations damped, but also the shape of the 300 °C-film spectrum changed significantly. This modification is due to the formation of Cu_2Se. Moreover, the transmittance spectrum of Cu_2Se [36] is similar to that of the 300 °C-film in figure 12(b).

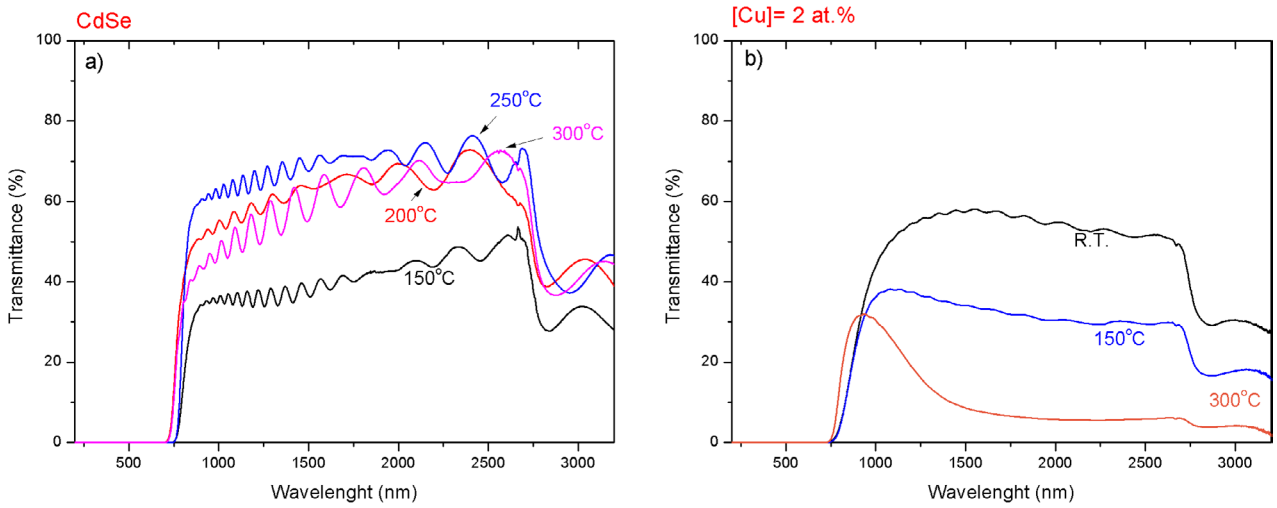

Figure 12. Optical transmission spectrum of films of (a) pure CdSe and (b) copper doped CdSe films with [Cu] = 2 at.% in the target. The strong absorption observed in all spectra starting at ~2750 nm is due to the substrate (glass).

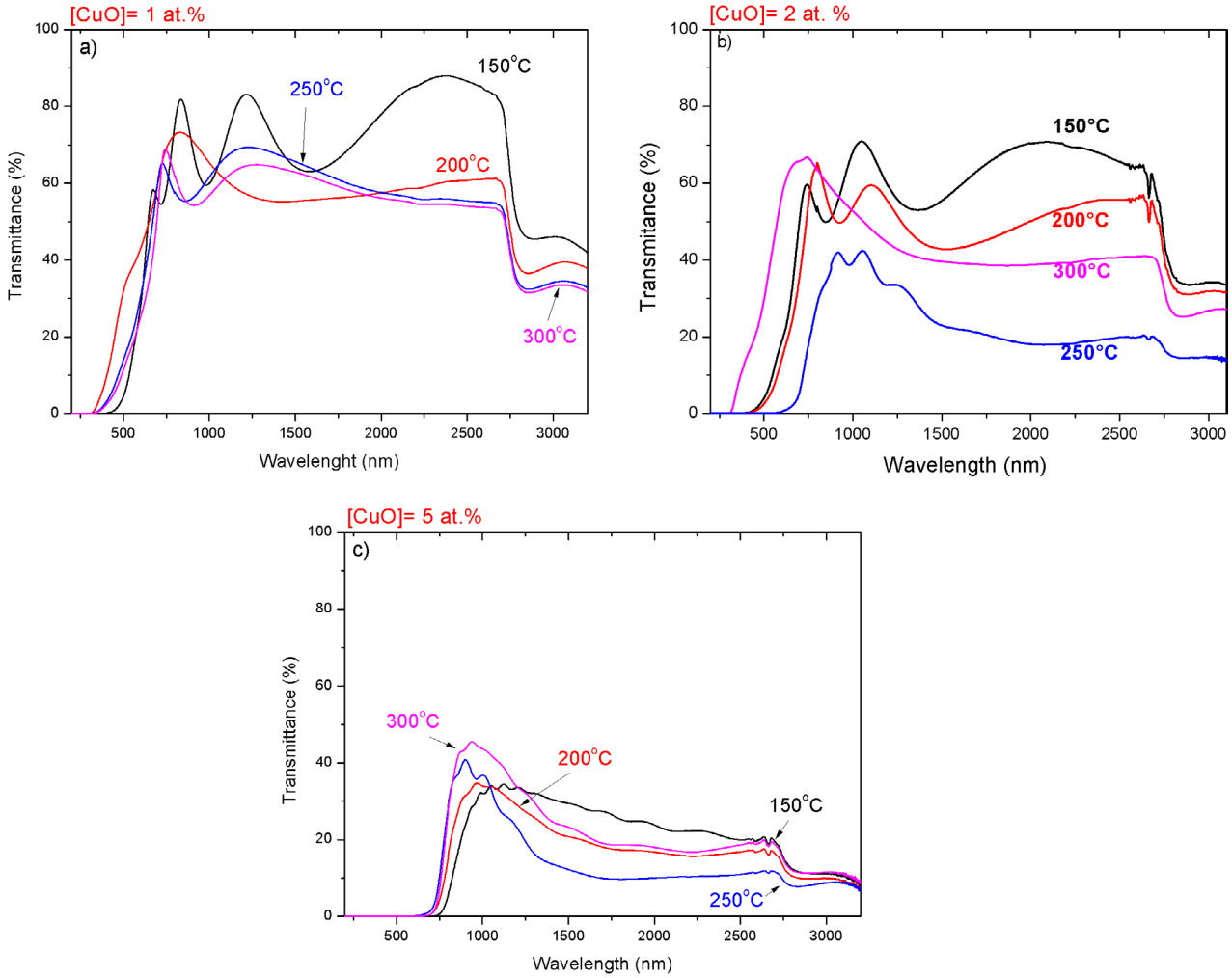

Figure 13. Optical transmission spectra of CdSe:Cu:O films grown with different concentrations of CuO in the target: (a) [CuO] = 1 at.%, (b) [CuO] = 2 at.%, and (c) [CuO] = 5 at.%. The strong absorption starting at ~2750 nm is due to the substrate (glass).

For concentrations of 1 at.% of CuO, figure 13(a), the mean transmittance was between 60% and 80%. The spectra were similar among them with no significant influence of their thickness. The oscillations due to interference effects are more noticeable in the spectrum of the 150 °C-film because it is ~3 times thicker than the others, figure 8. For 2 at.% of CuO in the target, figure 13(b), the effect on the electronic properties of the films due to the formation of Cu_2Se is clearly

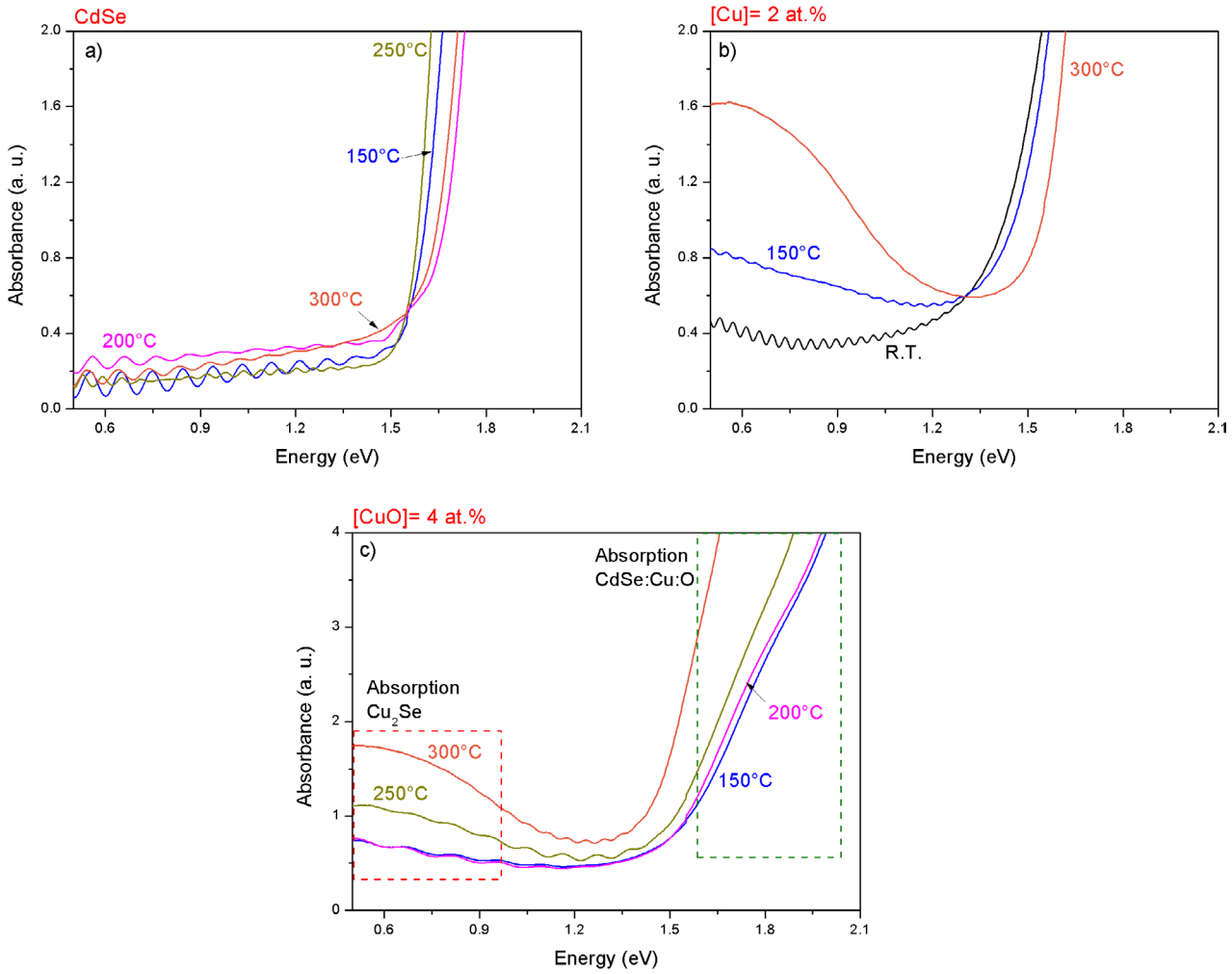

Figure 14. Optical absorption spectrum of films of (a) pure CdSe, (b) [Cu] = 2 at.%, and (c) [CuO] = 4 at.% in the target.

observable. The overall transmission is reduced and the higher the temperature, the more absorbent the film becomes (the 300 °C-film has the lowest thickness of this batch, figure 8). This characteristic agrees with the formation of Cu_2Se clusters in the films: the higher the substrate temperature, the higher the concentration of Cu_2Se. This is a general feature about the dependence of the formation of copper diselenide on substrate temperature in all films. The strong influence on the films transmittance of Cu_2Se is also evident in the samples grown with [CuO] = 5 at.%, figure 13(c), where the optical properties of the films are dominated by the Cu_2Se formations in the films.

The absorbance spectra of CdSe, CdSe:Cu and CdSe:Cu:O, with [CuO] = 4 at.%, are shown in figure 14 as a function of energy. In the case of the undoped CdSe films, figure 14(a), losses due to reflectivity, surface dispersion and absorption due to defects affect the below-band-gap (BBG) region so that absorbance differs from zero for energies smaller than E_g. In fact, the BBG absorbance for the CdSe films is between 0.1 and 0.3. In most cases, the BBG absorbance does not affect the determination of E_g when Tauc's model is employed because the linear extrapolation of the highly absorbent region to the energy axis is basically unaffected. In the case of the doped films presented in this work, the BBG absorbance can be as high as 1.6 for the Cu-doped (figure 14(b)), or 1.8 for the dual-doped (figure 14(c)) films. The strong BBG absorbance in doped films correlates with the presence of Cu_2Se clusters, thus, it may be ascribed to copper selenide particles immersed in the doped CdSe matrix. The optical measurements (transmission and absorbance) of our films are the result of the optical properties of the copper selenide particles and the doped CdSe matrixes.

For the band gap determination, it is noted that the overlap between the two types of absorbances (Cu_2Se and CdSe:Cu:O) is not significant, so that the determination of E_g for the dual-doped CdSe matrix is not affected when Tauc's method is employed. The model is described by the following relation [37]:

$$\alpha h\nu = B(h\nu - E_g)^n \tag{5}$$

where $h\nu$ is the photon energy and α is the absorption coefficient. The band gap was determined from the intersection on the energy axis in plots of $(\alpha h\nu)^n$ versus $h\nu$ ($n = 1/2$ or 2 for polycrystalline or amorphous films). The values of E_g are presented in figure 15 as a function of the substrate temperature. The band gap for undoped CdSe samples fluctuates slightly around 1.5 eV, regardless of the values of T_s. The band gap for cubic and hexagonal CdSe has been reported as 1.74 and

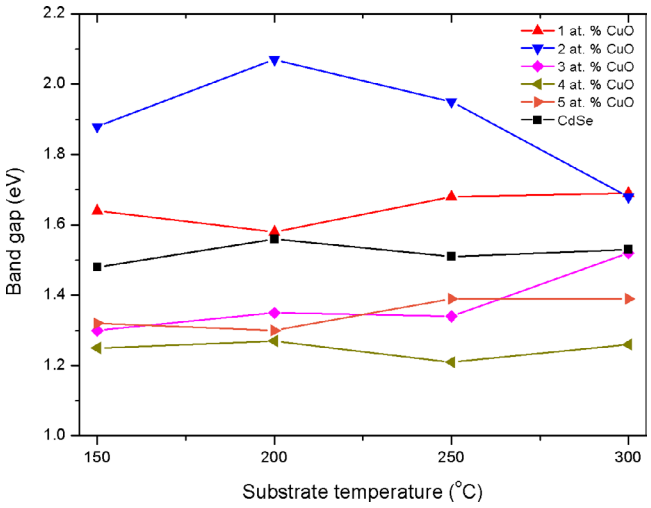

Figure 15. Band gap values of CdSe:Cu:O films as a function of substrate temperature for different concentrations of CuO in the target.

1.73 eV [38], respectively. Thus, different relative proportions of these phases in the films would not affect importantly the value of the band gap.

The values of E_g for the dual-doped CdSe films does not follow a single trend, figure 15. On the one hand, the band gap decreased with increasing the CuO concentration for 3, 4 and 5 at.%. The reason for this could be the formation of additional energy levels within the band gap as a consequence of doping. Similar observations have been described in doped CdSe films. Kriti *et al* [7] reported a decrease in the value of the band gap in Cu doped CdSe films. Additionally, works by Santhosh *et al* [10] and Mazhar Ali *et al* [5] determined a decrease in the band gap as a function of the concentration of Bi (1.67–1.65 eV) and Sb (1.69–1.68 eV), respectively. On the other hand, in our case doped films with 1 and 2 at.% of CuO in the target present the largest values for E_g; these are significantly larger than those of undoped CdSe. A correlation exists between the values of E_g and the crystallite size for these samples (table 1), in the sense that the crystallite size is the smallest for these films, while having the largest values of E_g, figure 15. This corresponds to the onset of quantum size effects, as the responsible mechanism for the appearance of values of E_g larger than that of bulk CdSe.

3.6. Electrical properties

The resistivity of the films was measured using the four-point-probe method. Table 2 shows the resistivity for films with CuO concentrations of 2, 3 and 5 at.%. Undoped CdSe films could not be measured because of their high resistivity, which has been reported to be around 10^6 Ω cm [39]. For the same reason, the resistivity of films with concentrations of 1 at.% CuO could not be obtained.

In general, the values of resistivity decreased for films where the formation of Cu_2Se (a material of low electrical resistivity ~10^{-4} Ω cm), was favored. It is interesting to note that, even though the film grown with 2 at.% at 150 °C is amorphous (figure 5), its resistivity is around 3 Ω cm, and

Table 2. Resistivity of dual doped CdSe:Cu:O films with concentrations in the target of [CuO] = 2, 3 and 5 at.%.

	Resistivity (Ω cm)		
Temperature (°C)	[CuO] = 2 at.%	[CuO] = 3 at.%	[CuO] = 5 at.%
150	3.15	[a]	3.87×10^1
200	4.15×10^{-1}	2.08×10^3	2.80
250	2.24×10^{-1}	[a]	[a]
300	9.6×10^{-1}	1.52×10^3	[a]

[a] Indicates films where no reliable contacts could be attained.

that polycrystalline films with 3 at.% CuO in the target have resistivities of the order of 10^3 Ω cm. In the former case, the structural disorder does not preclude having high conductivity (for an amorphous material); in the latter, the conductivity is improved with respect to pure CdSe, but it worsens with respect to that of films with 2 at.%. When the amount of CuO in the target increased to 5 at.%, the conductivity improves again with respect to the 3 at.% case. The electrical properties of the films are the result of competing and complex factors such as the structural quality, the existence of highly conducting Cu_2Se clusters in the CdSe host, and of free carrier scattering produced by these conditions.

4. Conclusions

The structural, optical and electrical properties of CdSe, CdSe:Cu and CdSe:Cu:O films deposited by RF sputtering have been studied. It was determined that the dopant concentration and crystalline characteristics, defined by the growth conditions, have a strong influence on the physical properties of the CdSe:Cu:O films. According to the x-ray diffraction analysis, undoped and copper-doped films were polycrystalline. Crystallite size in undoped films remained basically constant regardless of the substrate temperature. When copper was used as dopant, the crystallite size had a slight reduction. In the case of 1 and 2 at.% CdSe:Cu:O films, however, significant structural disorder was introduced. This tendency ceased when the substrate temperature increased. Well defined diffraction peaks related to CdSe and Cu_2Se were observed in samples grown at 300 °C for 2 at.% CuO in the target. At 3, 4 and 5 at.% all films were polycrystalline throughout the whole temperature range. The appearance of Cu_2Se clusters was favored by the increase of CuO in the target and by using high substrate temperatures. In-depth homogeneity was verified through grazing-angle x-ray diffraction experiments. In the Raman spectra of the CdSe, CdSe:Cu and CdSe:Cu:O films, the optical longitudinal mode of CdSe was observed, as well as its second and third harmonics, in agreement with the crystalline quality evidenced through x-ray diffraction experiments. The electronic properties of CdSe, namely optical and electrical, were strongly modified by the incorporation of Cu and O. An important reduction in the transmittance was observed, which became more significant as the deposition temperature and concentration of CuO in the target were raised. The band gap of the films was estimated using Tauc's method, finding

values between 1.21 and 2.07 eV. That is, the films' band gaps were above and below that of undoped CdSe. In the former case, there is correlation with the crystallite size indicating the existence of quantum size effects. In the latter, the lower values of E_g can originate from absorption processes produced by dopant-related electronic levels within the CdSe band gap. The electrical characterization showed that the CdSe:Cu:O films have resistivities between 2.08×10^3 and 9.6×10^{-1} Ω cm. In summary, our results showed that the incorporation of Cu and O in CdSe allowed the growth of sputtered films in a simple manner, and that it is possible to achieve control over the optical and electrical properties through variations in the growth conditions such as substrate temperature and relative concentration of CuO in the target.

Acknowledgments

The authors acknowledge the partial financial support from Conacyt-Mexico (Conacyt-SEP Ciencia Básica) through grant No. 257166 and from FOINS-CONACYT grant No. 2016-01-2488. N Navarro López acknowledges the PhD scholarship from Conacyt-Mexico.

ORCID iDs

Francisco Javier Flores-Ruiz https://orcid.org/0000-0002-8445-4223
Sergio Jiménez-Sandoval https://orcid.org/0000-0002-2143-3759

References

[1] Loizos Z, Mitsis A, Spyrellis N, Froment M and Maurin G 1993 Cadmium chalcogenide semiconducting thin films prepared by electrodeposition from boiling aqueous electrolytes *Thin Solid Films* **235** 51–6
[2] Bhargava R 1997 *Properties of Wide Bandgap II–VI Semiconductors* (London: INSPEC, Institute of Electrical Engineers)
[3] Chate P A, Patil S S, Patil J S, Sathe D J and Hankare P P 2012 Nanocrystalline CdSe: structural and photoelectrochemical characterization *Electron. Mater. Lett.* **8** 553–8
[4] Bao Z, Yang X, Li B, Luo R, Liu B, Tang P, Zhang J, Wu L, Li W and Feng L 2016 The study of CdSe thin film prepared by pulsed laser deposition for CdSe/CdTe solar cell *J. Mater. Sci., Mater. Electron.* **27** 7233–9
[5] Mazhar A, Waqar A A S, Zubair M, Nazar A S and Arshad M 2013 Physical properties of Sb-doped CdSe thin films by thermal evaporation method *Appl. Surf. Sci.* **284** 482–8
[6] Li C, Wang F, Chen Y, Wu L, Zhang J, Li W, He X, Li B and Feng L 2018 Characterization of sputtered CdSe thin films as the window layer for CdTe solar cells *Mater. Sci. Semicond. Process.* **83** 89–95
[7] Sharma K, Al-Kabbi A, Saini G S S and Tripathi S K 2012 Effect of Cu incorporation on structural and optical properties of nanocrystalline CdSe (nc-CdSe:Cu) thin films *J. Alloys Compd.* **540** 198–203
[8] Wageh S, Al-Ghamdi Ahmed A, Al-Zahrani A A and Hafedh Driss 2019 High quantum yield Cu doped CdSe quantum dots *Mater. Res. Express* **6** 0850d4
[9] Bao Z, Liu L, Yang X, Tang P, Yang K, Lu H, He S, Liu J, Liu X and Li B 2017 Synthesis and characterization of novel oxygenated CdSe window layer for CdTe thin film solar cells *Mater. Sci. Semicond. Process.* **63** 12–7
[10] Santhosh T C M, Kasturi V B and Shivakumar G K 2017 Effect of Bi doping on the properties of CdSe thin films for optoelectronic device applications *Mater. Sci. Semicond. Process.* **68** 114–7
[11] Jiménez Sandoval S, Garnett Ruiz G E, Santos Cruz J, Jiménez Sandoval O, Torres Delgado G, Castanedo Pérez R and Morales Sánchez E 2006 Band gap tuning and high electrical conductivity in amorphous and polycrystalline films of the $Cu_x(CdTe)_yO_z$ system *J. Appl. Phys.* **100** 113713
[12] Carmona Rodríguez J, Lozada Morales R, del Angel Vicente P, Jiménez Sandoval O, López Calzada G, Dahlberg D and Jiménez Sandoval S 2011 Properties of $Cu_x(CdTe)_yO_z$ thin films: composition-dependent control of band gap and charge transport *J. Mater. Chem.* **21** 13001–8
[13] Berumen Torres J A, Beristain Bautista A, Rodríguez Melgarejo F, Hernández Landaverde M A, López Calzada G, Araiza J J and Jiménez Sandoval S 2016 Properties of ZnO–Cu_{2-x}Se thin films deposited by sputtering from composite ZnSe–Cu_2O targets *Opt. Mater. Express* **6** 2812–23
[14] Arreola Jardón G, Jiménez Sandoval S and Mendoza Galván A 2014 Growth and characterization of CuCdTeO thin films sputtered from CdTe–CuO composite targets *Vacuum* **101** 130–5
[15] Mendoza Galván A, Arreola Jardón G, Karlsson L H, Persson P O A and Jiménez Sandoval S 2014 Optical properties of CuCdTeO thin films sputtered from CdTe–CuO composite targets *Thin Solid Films* **571** 706–12
[16] Beristain Bautista A, Olivos E, Arroyave R, Rodríguez Melgarejo F and Jiménez Sandoval S 2018 Influence of deposition temperature on the properties of sputtered films grown from a Cu_2O–CdO–TeO_2 composite target: Electronic properties of $CdTe_2O_5$ *Superlattices Microstruct.* **123** 403–13
[17] Love G, Scott V D, Dennis N M T and Laurenson L 1981 Sources of contamination in electron optical equipment *Scanning* **4** 32–9
[18] Pathinettam Padiyan D, Marikani A and Murali K R 2003 Influence of thickness and substrate temperature on electrical and photoelectrical properties of vacuum-deposited CdSe thin films *Mater. Chem. Phys.* **78** 51–8
[19] Mathuri S, Ramamurthi K and Ramesh Babu R 2017 Influence of deposition distance and substrate temperature on the CdSe thin films deposited by electron beam evaporation technique *Thin Solid Films* **625** 138–47
[20] Nair M T S and Nair P K 1993 Enhancement of photosensitivity in chemically deposited CdSe thin films by air annealing *J. Appl. Phys.* **74** 1879–84
[21] Klug H P and Alexander L E 1974 *X-Ray Diffraction Procedures for Polycrystalline and Amorphous Materials* 2nd edn (New York: Wiley)
[22] Khorsand Zak A, Abd Majid W H, Abrishami M E and Yousefi R 2011 X-ray analysis of ZnO nanoparticles by Williamson–Hall and size-strain plot methods *Solid State Sci.* **13** 251–6
[23] Williamson G K and Smallman R E 1956 Dislocation densities in some annealed and cold-worked metals from measurements on the x-ray Debye-Scherrer spectrum *Phil. Mag.* **1** 34–46
[24] Ivanova T, Harizanova A, Koutzarova T and Vertruyen B 2010 Study of ZnO sol-gel films: Effect of annealing *Mater. Lett.* **64** 1147–9
[25] Caglar Y, Ilican S, Caglar M, Yakuphanoglu F, Wu J, Gao K and Lu P 2009 Influence of heat treatment on the nanocrystalline structure of ZnO film deposited on p-Si *J. Alloys Compd.* **481** 885–9

[26] Suthan Kissinger N J, Jayachandran M, Perumal K and Sanjeeviraja C 2007 Structural and optical properties of electron beam evaporated CdSe thin films *Bull. Mater. Sci.* **30** 547–51

[27] Syed Basheer Ahamed M G, Balu A R, Nagarethinam V S, Thayamanavan A, Murali K R, Sanjeeviraja C and Jayachandran M 2010 Structural, optical and electrical properties of electron beam evaporated CdSe thin films *Cryst. Res. Technol.* **45** 387–92

[28] Ramirez-Bon R, Espinoza-Beltran F J, Arizpe-Chavez H, Zelaya Angel O and Sanchez Sinencio F 1996 Structural and optical studies in a-CdTe:O annealed films *J. Appl. Phys.* **79** 7682–7

[29] Carmona Rodríguez J, Lozada Morales R, Jiménez-Sandoval O, Rodríguez Melgarejo F, Meléndez Lira M and Jiménez Sandoval S 2008 $CdTeO_x$ to $CdTeO_3$ structural phase transition in as-grown polycrystalline films by reactive sputtering *J. Appl. Phys.* **103** 123516

[30] Lide D R 2005 *CRC Handbook of Chemistry and Physics* 85th edn (Boca Raton, FL: CRC Press)

[31] Deshpande M P, Garg N, Bhatt S V, Sakariya P and Chaki S H 2013 Characterization of CdSe thin films deposited by chemical bath solutions containing triethanolamine *Mater. Sci. Semicond. Process.* **16** 915–22

[32] Purohit A, Chander S, Nehra S P and Dhaka M S 2015 Effect of air annealing on structural, optical, morphological and electrical properties of thermally evaporated CdSe thin films *Physica* E **69** 342–8

[33] Yeh C Y, Lu Z W, Froyen S and Zunger A 1992 Zinc-blende-wurtzite polytypism in semiconductors *Phys. Rev.* B **46** 10086–97

[34] Cusco R, Consonni V, Bellet-Amalric E, André R and Artús L 2017 Phase discrimination in CdSe structures by means of Raman scattering *Phys. Status Solidi RRL* **5** 1700006

[35] Ichimura M, Takeuchi K, Nakamura A and Arai E 2001 Photochemical deposition of Se and CdSe films from aqueous solutions *Thin Solid Films* **384** 157–9

[36] Ahn H and Um Y 2014 Thickness dependences of the structural, optical and electrical properties of Cu_2Se thin films grown by using DC magnetron sputtering *J. Korean Phys. Soc.* **64** 1600–4

[37] Sharma K, Al-Kabbi A, Saini G S S and Tripathi S K 2015 Influence of Zn doping on structural, optical and electrical properties of nanocrystalline CdSe thin films *J. Alloys Compd.* **651** 42–8

[38] Ninomiya S and Adachi S 1995 Optical properties of cubic and hexagonal CdSe *J. Appl. Phys.* **78** 4681–9

[39] Yadav A A, Barote M A and Masumdar E U 2010 Studies on cadmium selenide (CdSe) thin films deposited by spray pyrolysis *Mater. Chem. Phys.* **121** 53–7